EXPERIMENTAL AND NUMERICAL INVESTIGATION OF THE UNIAXIAL COMPRESSION BEHAVIOR OF SRG-JACKETED R/C COLUMNS

Antonios A. Katsamakas [1], Vassilis K. Papanikolaou [2], Georgia E. Thermou [3] and Konstantinos Katakalos [4]

[1] PhD candidate, Chair of Seismic Design and Analysis, DBAUG, ETH Zurich, Zurich, CH-8093, Switzerland (katsamakas@ibk.baug.ethz.ch)

[2]Assistant Professor, School of Civil Engineering, Aristotle University of Thessaloniki, Thessaloniki, GR-54124, Greece. (billy@civil.auth.gr)

[3]Assistant Professor in Structural Engineering, Civil Engineering Department., The University of Nottingham, Nottingham, NG7 2RD, UK. (georgia.thermou@nottingham.ac.uk)

[4]Assistant Professor, School of Civil Engineering, Aristotle University of Thessaloniki, Thessaloniki, GR-54124, Greece. (kkatakal@civil.auth.gr)

Abstract

This paper presents an experimental and numerical investigation of Reinforced Concrete (R/C) short columns strengthened with Steel Reinforced Grout (SRG) jackets. Nine specimens were constructed and tested under concentric monotonic uniaxial compression, measuring compressive force, axial and lateral displacements. Parameters of investigation were the influence of internal steel reinforcement (i.e. no reinforcement, sparse or dense stirrups) and the number of the

externally applied SRG jackets (i.e. one or two layers). Subsequently, a three-dimensional finite element methodology was developed, aiming to predict the response of those specimens. Experimental results show that the strength and deformation capacity of the specimens was significantly enhanced with the addition of the SRG jackets, since the strengthening schemes provided sufficient passive confinement. The comparison between experimental and numerical results, in terms of failure mode, axial and lateral stress-strain curves, demonstrated satisfying correlation, proving the efficiency of the proposed numerical model.

Keywords SRG; textiles; finite elements; strengthening; composite materials; confinement; columns; reinforced concrete.

1. INTRODUCTION

With a large proportion of Reinforced Concrete (R/C) structures worldwide built without or with inadequate seismic code provisions, the need for retrofitting becomes imperative. This led to the development of composite materials, such as Fiber Reinforced Polymers (FRPs) [1-24], used as externally bonded reinforcement. The favorable properties of FRPs, such as their easy and fast application, high strength-to-weight ratio and corrosion resistance, led to their widespread use in retrofitting applications of Reinforced Concrete (R/C) structures. Nevertheless, organic binders (e.g., epoxy resins), which are used to bond the FRP jackets to the concrete members, are linked to several drawbacks, such as poor behavior in elevated temperatures, insufficient application on wet surfaces and lack of vapor permeability. To alleviate those disadvantages, the replacement of organic binders with inorganic ones was proposed, leading to a new generation of inorganic composite materials, the Fiber-Reinforced Cementitious Matrix (FRCM) [e.g., 25-40]. Steel Reinforced Grout (SRG), which belongs in FRCM family of materials, is a composite system comprising high-strength steel textiles embedded in cementitious grout [41-62].

SRG jackets were applied as a confinement material for concrete and R/C columns subjected to uniaxial compression or under combined axial loading and cyclic lateral displacement reversals, demonstrating the efficiency of this retrofitting scheme in increasing strength and deformation capacity [41-49]. When a concrete column is subjected to compression, external jackets operate similarly to conventional stirrups; the lateral dilation of concrete activates the jacket, which provides passive confinement stresses.

Previous studies of SRG-confined plain concrete and R/C columns identified critical design and manufacturing parameters that influence the confinement efficiency, such as the concrete strength, the internal steel reinforcement, the density of the steel fabric, the strength of the inorganic matrix, the anchorage length, the number of layers and the construction details (e.g.,

rounded or sharp edges of the cross-section) [43-44, 48-49]. When debonding of the jacket is avoided (i.e., a low-density jacket and sufficient anchorage is employed), experimental results showed that increasing the number of layers of SRG jacket increases the efficiency of the retrofitting [46]. Moreover, the effectiveness of the retrofitting scheme is improved as the unconfined concrete strength decreases and the strength of the SRG mortar increases [48]. The influence of the corner radius for SRG systems was investigated by Thermou et al. [44], proving that the effectiveness of the SRG jacketing system improved as the corner radius increased. For SRG-strengthened specimens, the ratio r/b is utilized to quantify the corner radius effect, where r is the radius of the corner, and b is the length of the cross-section. It was proved that, for low-density textiles, using an r/b ratio close to 0.35 is sufficient [44]. Similar conclusions regarding the corner radius were drawn for specimens retrofitted with Textile Reinforced Mortar (TRM). A review by Koutas et al. [32] concluded that, for TRM-retrofitted specimens, the radius (r) should be equal to, or larger than, $0.1b$ or 25 mm.

Three different failure modes dominate the response of SRG-confined R/C columns when these are subjected to uniaxial compression [48]: (a) debonding of the jacket at the termination of the anchorage length, (b) tensile fracture of the steel cords of the fabric due to excess of their tensile strength, and, (c) partial debonding, which is a combination of the two aforementioned failure modes. It was observed that increasing the density of the textile promotes debonding due to insufficient penetration of the mortar and incomplete pre-bending of the steel textile. Overall, using a dense steel textile, a low-strength mortar or a short overlap length promotes debonding of the SRG jacket. Contrariwise, using a low-density textile, a high-strength mortar or a jacket with sufficient overlap length promotes rupture of the textile [43, 48]. In a previous experimental study [44], the influence of the cross-section shape of the retrofitted column was assessed. The effectiveness of the SRG jacketing system was improved when the cross-section had rounded edges and as the radius increased. This is because in members with rectangular sections and high-

density textiles, fracture may initiate at one of the corners due to stress concentration. However, when low-density steel textiles are used, the gain in compressive strength is significant even for specimens with sharp edges. This is due to the low axial stiffness of the low-density textile, which results in low stress concentration in the region of the corners, with the inorganic matrix facilitating stress distribution at this area. In a preliminary study [49] the effect of the loading rate on the axial compressive behavior of concrete columns was investigated, observing that a dynamic application of compressive loads could lead to strength decrease. All the aforementioned studies on SRG-confined columns concluded that the presence of the jacket does not modify the initial stiffness but mainly affects the post-elastic behavior of the specimen.

The first part of this paper aims to build on the existing experimental applications of SRG-confined plain concrete and R/C columns. Enriching this database is important since the experimental results are influenced by parameters such as the internal steel reinforcement, the density of the textile, the geometry of the specimen, and the construction details (e.g., radius of corner of cross-section, loading rate, and overlap length). Aiming at the widespread use of SRG as a retrofitting material, these parameters need further clarification.

The second part of this paper proposes a numerical methodology for modeling SRG-confined R/C members. Three-dimensional finite elements are employed, together with advanced constitutive laws for the involved materials (i.e., concrete, steel and SRG). Embedded truss elements were used to simulate the individual steel cords of SRG. This approach promotes time-efficiency, is consistent with the physical problem and has already shown promising results in previous applications, where it captured the response of SRG-retrofitted shear-critical R/C beams [62]. The present paper extends the above methodology to SRG-confined R/C columns. Moreover, to the best of the authors' knowledge, the present paper is the first one to model SRG-confined R/C columns using three-dimensional finite elements.

2. EXPERIMENTAL INVESTIGATION

2.1 Specimen Details

Nine column-type specimens were tested: three plain concrete and six reinforced concrete (R/C) specimens. All specimens were constructed using the same concrete mix, having a 200 mm square cross-section and a height of 380 mm. Parameters of investigation were the amount of transverse steel reinforcement (i.e. no reinforcement, 200 mm or 100 mm stirrup spacing) and the number of SRG layers (i.e. one or two). The objective of the experimental study is to quantify the ability of the jacketing schemes to increase the strength and deformation capacity of the specimen and to estimate the correlation between the efficiency of the jacketing scheme and the amount of steel reinforcement. The prisms were divided into three groups, with three identical specimens in each one. The first group comprised plain concrete specimens (i.e., with no internal steel reinforcement, group U). The specimens of the other two groups (i.e., groups S200 and S100) were reinforced with four longitudinal 12 mm-diameter steel bars, placed at the corners of the section. The specimens of groups S200 and S100 had 8 mm-diameter stirrups placed every 200 mm and 100 mm, respectively (Figure 1). For the specimens of group S200 and S100, the corresponding s/d_b ratio is 16.67 and 8.33, respectively, where s is the stirrup spacing and d_b the diameter of the longitudinal rebar. Previous studies showed that when $s/d_b < 6$, inelastic buckling is expected to occur. Contrariwise, when $s/d_b > 10$, elastic buckling prior to yielding is observed. [63-67] Each group (of three specimens) included one control specimen (not retrofitted), one single-layered and one double-layered specimen. The specimen details are shown in Table 1.

Specimens were given the notation X_Y, where X indicates the group (i.e., group U, S200 or S100), and Y corresponds to the type of the jacketing system (i.e., C for the control specimens, S1 and S2 for the single- or double-layered specimens, respectively). For example, specimen S100_S2

corresponds to the specimen from Group S100 (dense stirrups), which was retrofitted with two layers of high strength steel textile.

Table 1. Summary of the internal steel reinforcement and the retrofitting scheme of the specimens.

Group	**Longitudinal Reinforcement**	**Transverse Reinforcement**	**Control Specimen**	**Specimen with *one* layer of SRG jacket**	**Specimen with *two* layers of SRG jackets**
U	-	-	U_C	U_S1	U_S2
S200	4Ø12	Ø8/200	S200_C	S200_S1	S200_S2
S100	4Ø12	Ø8/100	S100_C	S100_S1	S100_S2

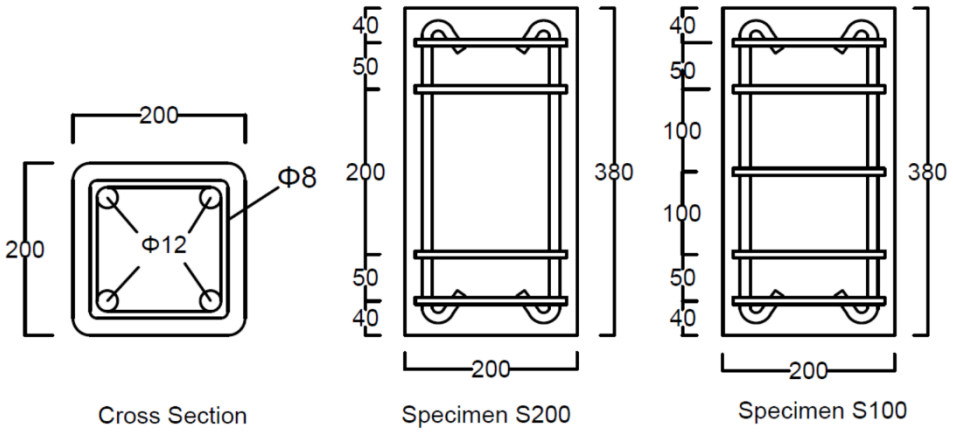

Figure 1. Dimensions and internal steel reinforcement configurations of specimens belonging to groups S200 and S100 (Dimensions are in mm).

2.2 Material properties

Concrete: All nine columns were constructed using the same concrete mix, which was cast in a single batch. The average concrete compressive strength, obtained from seven 150 mm-sided cubes at 28 days, was equal to f_{cm} = 24.10 MPa, with a standard deviation of 0.8 MPa (3.3%). The

maximum aggregate size was 8 mm. Three days after casting, the wooden molds were removed, the specimens were placed in a water tank, and left to cure in these humidity conditions for 28 days.

Steel: The steel grade used both for longitudinal and transverse steel reinforcement was B500C. The mechanical properties of the reinforcement steel were obtained from standard tensile tests, with the yield stress, the maximum stress, the yield strain, and the strain at maximum stress being equal to f_y = 587 MPa, f_{max} = 651 MPa, ε_y = 0.0029, and ε_{max} = 0.10, respectively.

SRG: Each layer of the SRG jacket consisted of Ultra High Tensile Stress Steel (UHTSS) textile and cementitious grout. The steel textile consisted of 3×2 type cords, meaning that each cord consists of five filaments: three straight and two more twisted around them (Figure 2). In the present study, the density of the textile was equal to 3.15 cords/cm (8 cords/inch) with an equivalent thickness of 0.169 mm (Figure 2). This textile is considered a medium-density one. Before the application, pre-bending of the steel textile to the desired dimensions is highly recommended to facilitate installation. A commercial one-component geo-mortar was used as the connecting matrix, the first layer applied in the concrete surface, and as a final cover. A critical parameter that affects the effectiveness of the retrofitting is the axial stiffness of the jacket, which is defined by the utilized steel textile. Axial stiffness, $K_{f,s}$, is equal to $K_{f,s} = t_s \times E_{f,s,}$ where t_s is the equivalent thickness per unit width of the steel textile, and $E_{f,s}$ is the elastic modulus of the steel cords. The equivalent thickness per unit width, t_s, is equal to $t_s = D_f \times A_{cord}$, where D_f is the density of the textile (cords/cm), and A_{cord} is the area of each cord (cm^2) (Table 2). The geometrical and mechanical properties of each cord, as provided by the manufacturer, appear in Table 3. The mechanical properties of the mortar appear in Table 4.

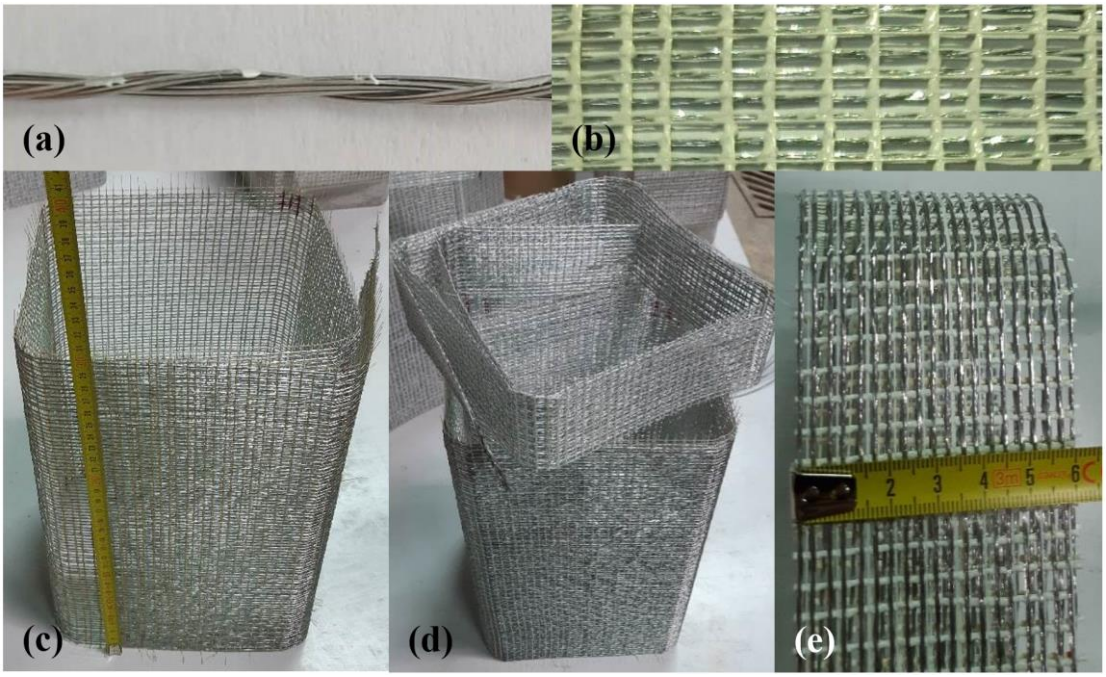

Figure 2. Steel cords of the SRG jacket. a) 3×2 type cords; b) Steel textile with a density of 3.15 cords/cm; c) pre-bent steel jacket in two pieces; d) bottom part of the pre-bent steel jacket; e) bottom part of the pre-bent steel jacket.

Table 2. Axial stiffness of the steel textiles utilized in the SRG jackets.

Elastic modulus, $E_{f,s}$ (GPa)	**Equivalent thickness t_s (mm)**	**Number of layers**	**Axial stiffness $K_{f,s}$ (kN/mm)**
190	0.169	1	31.6
		2	63.2

Table 3. Geometrical and mechanical properties of the cables used in the steel textiles, as provided by the manufacturer.

Cord diameter (mm)	**Cord area (mm^2)**	**Break load (N)**	**Tensile strength, $f_{fu,s}$ (MPa)**	**Strain to failure, $\varepsilon_{fu,s}$ (mm/mm)**	**Elastic modulus, E_f (GPa)**
0.827	0.538	1506	2800	0.015	190

Table 4. Mechanical properties of the mortar utilized in the SRG jackets, as provided by the manufacturer.

Modulus of elasticity, E_m (GPa)	**Flexural strength, f_{mf} (MPa)**	**Compressive strength, f_{mc} (MPa)**	**Adhesive bond strength, f_{mb} (MPa)**
25	10	55	2

2.3 Construction details

Before the application of the SRG jackets, the substrate of the specimens was roughened, cleaned, and saturated, aiming to improve the jacket-specimen bond. Subsequently, the first layer of cementitious grout was applied by hand to the surface of the specimens (Figure 3a) and the steel textile was placed afterwards (Figure 3b). The steel textiles were pre-bent and pre-cut before application, also considering the 20 mm corner radius of the cross-section, to facilitate installation. The height of a steel textile is equal to 300 mm; thus, two pieces of textile were utilized (with a height of 300 mm and 60 mm, respectively), leaving a 10 mm gap between the steel bearing plates of the loading machine and the steel textile, both on top and bottom of the specimen (it is recalled that the total height of the specimens was 380 mm). This 10 mm gap (both on top and bottom) was designed to avoid the direct loading of the jacketing scheme by the two loading plates [46]. The bottom jacket was placed first, and the upper one followed. The grout was squeezed out between the gaps of the steel textile by manually applied pressure. After the application of the textile to one full cycle, the remaining length was lapped over the lateral surface. The lap length of the external jacket was used as additional anchorage for the jacketing scheme and was equal to two sides of the specimen (i.e., 400 mm), similarly to [43, 44, 47]. In all specimens, the ends of the stirrups were rotated at 135^o angle (i.e., closed stirrups). The four corners of the concrete cover were rounded at a radius equal to 20 mm, corresponding to a ratio r/b = 0.1, as defined in section 1.

Following the application of the steel textile, a final coat of the cementitious grout was applied to the external surface (Figure 3c). The thickness of the grout layer was such as to guarantee that the steel textile was fully embedded in the cementitious grout ([46], among others). Each layer of SRG jacket was less than 10 mm thick in all applications.

Figure 3. Application of one layer of SRG jacket. a) Application of the first layer of grout; b) Application of the steel textile; c) Application of the second layer of grout; d) View of the retrofitted specimen before testing.

2.4 Description of the experimental setup

The specimens were tested under concentric monotonic uniaxial compression. The load was applied as prescribed displacement, at a rate of 0.01 mm/sec, using a compression machine with a maximum capacity of 6000 kN. The corresponding applied load, that is the reaction of the column to the prescribed displacement, was measured using a load cell with a maximum capacity of 2000 kN placed at the top of the specimens. Rigid steel plates were placed on the top and bottom of the tested specimens and thin plywood plates were inserted between those steel plates and the specimen, to alleviate any small top/bottom surface unevenness of the specimen.

Axial and lateral strains were measured using a custom-made measuring apparatus (Figure 4). This configuration comprised twelve (12) LVDTs, with three of them placed at each side of the tested specimen. Eight (8) LVDTs were utilized to measure axial displacements, and four (4) to measure lateral displacements. When the mortar of the SRG jacket hardened, the external surface was painted, and 12 screws (3 screws per side) were mounted to the concrete core, passing through the width of the SRG jacket (Figure 3d). These screws were later used to attach the Linear Variable Differential Transformers (LVDTs), to measure the axial and lateral displacements. Axial (vertical) displacement (Δv_i) for each side (i) of the specimen was calculated as the difference between the top and bottom mounting positions at 180 mm vertical distance. The average of the four sides provided the final axial displacement, which was then divided by the distance between the mounting positions ($\varepsilon_v = (\Sigma \Delta v_i/4)/180$ mm) to be converted to axial strain. The remaining four LVDTs were placed in the middle of the height of the column and measured the horizontal lateral displacement (Δh_i). The average of those four values was divided by half of the cross-section (200/2 = 100 mm) to provide the lateral strain ($\varepsilon_h = (\Sigma \Delta h_i/4)/100$mm). All LVDT cores were tied via strings on screws mounted to the concrete core, penetrating the jacketing layers. This allowed the direct measurement of the axial and lateral strain of the concrete core, with the measurements being unaffected from a possible jacket failure. The test setup appears in figure 4, whereas the experimental results appear in a subsequent section.

3. EXPERIMENTAL RESULTS

The typical response curve of the SRG-strengthened columns is characterized by three branches (Figure 5): i) An initial (elastic) ascending branch which is practically unaffected by the presence of the jacket and is therefore identical to all specimens. ii) The “yielding branch”, where the initial slope (axial stiffness) is reduced, and the specimen reaches its maximum strength. iii)

The “failure branch”, which may correspond to three distinct response modes: iii-a) For unretrofitted specimens (U_C, S200_C, S100_C) the point of maximum stress is close to the failure point. iii-b) For one-layered SRG jacketed specimens (U_S1, S200_S1, and S100_S1) the point of maximum strength corresponds to initiation of *debonding* of the SRG jacket. iii-c). For two-layered SRG jacketed specimens (U_S2, S200_S2, S100_S2), after the maximum strength is reached and debonding of the external layer initiates, confinement stresses are mainly transferred to the inner layer of the jacket.

Regarding the response of the longitudinal steel reinforcement bars, three different levels are conventionally defined to describe the buckling level at the end of the test. “No buckling” is used for bars that remained straight (180 degrees) after the end of the test, “moderate buckling” is used for bars whose final inclination was between 180 and 210 degrees, and “intense buckling” is used for bars that buckled more than 210 degrees (Table 5).

*Control specimens***:** Specimens U_C, S200_C, and S100_C failed due to concrete cracking in the middle of the height of the specimen; a typical failure mode for concrete specimens subjected to uniaxial compression (Figures 6a, 7a, 8a). The maximum strength of the specimens was 27.4 MPa, 29.6 MPa and 29.4 MPa for specimens U_C, S200_C, and S100_C, respectively (Figure 5) (recall that the mean cylinder strength was f_{cm} = 24.10 MPa). Specimen U_C demonstrated a brittle failure mode, with concrete spalling mainly concentrated in one of the four sides of the specimen. The same crack pattern was observed in specimen S200_C, where moderate bar buckling was also observed. In specimen S100_C, cracks were more distributed, and inelasticity was mainly concentrated in the middle of the height of the column. The overall response of specimen S100_C is ductile in comparison to specimens U_C and S200_C due to the densely placed stirrups (Figure 5).

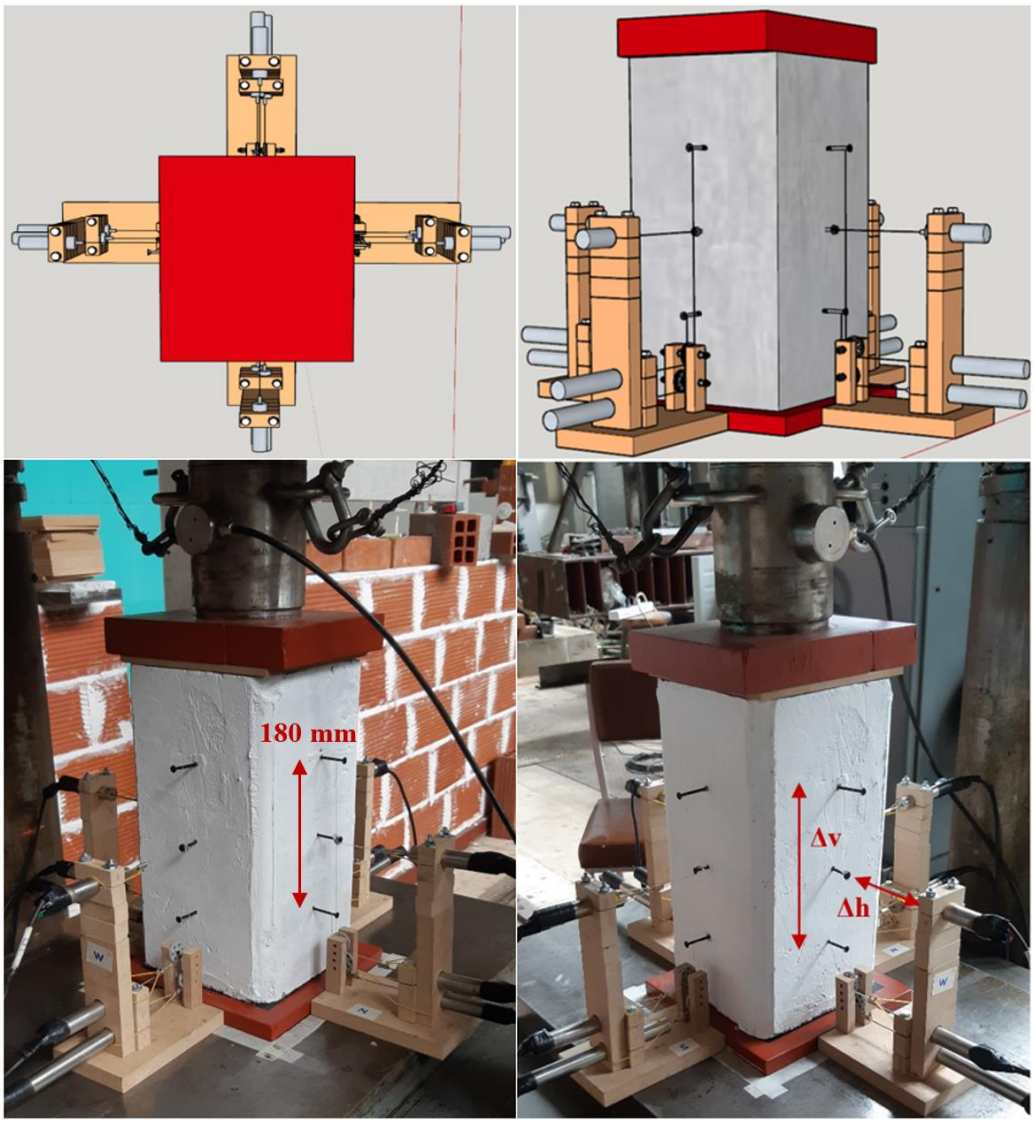

Figure 4. Top: 3D sketch of the experimental setup, comprising 12 LVDTs; Bottom: view of the setup during the experimental procedure.

The specimens retrofitted *with one layer of SRG jacket* (U_S1, S200_S1 and S100_S1) demonstrated a semi-ductile failure mode with debonding of the jacket and failure of the concrete core. When specimens reached their maximum load (30.6 MPa, 31.6 MPa and 31 MPa, respectively), debonding of the SRG jacket was observed, resulting in a significant load drop (Figure 5). Debonding was evident at the end of the lap length (Figures 6b, 7b, 8b). The softening branch was mildly declining, whereas failure was reached at a higher strain value. (Figure 5). Even

though load increased in these specimens (due to the retrofitting scheme), only moderate buckling of the longitudinal reinforcement was observed (Figure 7c, 8c).

The specimens retrofitted *with two layers of SRG jacket* **(**U_S2, S200_S2 and S100_S2) demonstrated a ductile behavior, while the SRG jacketing system failed in a mixed mode of failure. Specifically, debonding occurred at the external SRG layer, whereas the internal layer failed due to fracture of the steel cords. When the specimens reached their maximum strength (31.5 MPa, 35.1 MPa and 35.8 MPa, respectively, Figure 5), the external layer of SRG failed due to debonding. Hence, for the utilized textile density (3.15 cords/cm), an anchorage length equal to 2 sides of the specimen (i.e., 400 mm) is unable of preventing debonding. A future solution could be using a larger anchorage length (e.g., equal to 3 sides of the cross section), or developing additional mechanical measures. Failure of the specimens (ultimate point of the response) occurred when the inner SRG layer reached its maximum tensile stress, where fracture of the cords was observed (Figure 7d, 8d). The presence of the stirrups in specimens S200_S2 and S100_S2 led to a more ductile failure mode in comparison to specimen U_S2. Both specimen S200_S2 and specimen S100_S2 demonstrated significant buckling of the longitudinal steel reinforcement (Figures 7e, 8e). Previous studies [8,46] demonstrated that reinforcement buckling creates additional concentrated stresses in the perimeter, thus promoting debonding of the externally bonded jacketing system. Therefore, even though external bonded composites can increase strength and deformation capacity, and delay bar buckling, they cannot exclude it. Similar conclusions were also drawn in the past for FRP-retrofitted R/C columns [8].

The lateral stress-strain diagrams were similar to the axial ones, following the various significant points and main conclusions. More specifically, they comprise an initial (elastic) branch that is mainly governed by the Poisson's ratio, with the lateral strain maintaining low values, equal to approximately 0.2 of the axial strain. For most specimens, the end of the initial branch coincides with the point of maximum strength, which is reached at a lateral strain level of 0.5-0.6 ‰. These

levels of lateral strain are comparable to the ones observed by Tastani et al. [8]. Subsequently, these specimens fail, and the lateral strain increases substantially, up to failure, which corresponds to a lateral strain level of 5-10 ‰. In specimens with two layers of SRG jacket, the end of the initial branch is not the point of maximum strength, but the starting point of a plateau of lateral strain, similar to the one of the axial strain.

To quantify the strength and ductility gain from each retrofitting scheme, three indexes were defined. Each retrofitted specimen (U_S1, U_S2, S200_S1, S200_S2, S100_S1, and S100_S2), was compared to the control specimen of the corresponding group (U_C, S200_C, and S100_C). The first index is strength increase, which was the increase of the maximum measured stress in each specimen. The second is the axial strain ratio ($\varepsilon_{ult} / \varepsilon_{max}$), which was defined as the ratio of the ultimate axial strain (ε_{ult}) divided by the axial strain in the maximum load (ε_{max}). The last one is the energy increase, which is equal to the increase in the area below the stress-strain curve. Table 6 shows the efficiency of each strengthening configuration based on the aforementioned indexes.

Specimens retrofitted with one layer of SRG jacket demonstrated a moderate strength increase, a high increase of axial strain ratio ($\varepsilon_{ult} / \varepsilon_{max}$) and moderate energy increase (Table 6). Columns retrofitted with two layers of SRG jacket (U_S2, S200_S2, and S100_S2) were able of receiving significantly higher load, whereas the increase in terms of axial strain ratio ($\varepsilon_{ult} / \varepsilon_{max}$) and dissipated energy was substantial (Table 6). All three indexes show that the specimens retrofitted with two layers of SRG jacket perform significantly better than the specimens retrofitted with one layer of SRG jacket. Moreover, the values of the axial strain ratio ($\varepsilon_{ult} / \varepsilon_{max}$) and the energy increase were higher in comparison to the strength increase. Focusing on the index of energy increase, it is observed that, as the internal steel reinforcement of the columns increases, the energy increase due to the retrofitting becomes less significant. This implies that, in specimens with dense stirrups, the additional confinement due to the retrofitting is not expected to

substantially improve the overall response. The aforementioned effects explain the limited strength and energy increase of specimen S100_S1, in comparison to the significant-to-substantial increase of the other specimens (Table 6).

A summary of the experimentally observed failure modes of the SRG jackets and the longitudinal steel reinforcement is presented in Table 5, whereas a summary of the strength and ductility increase due to the retrofitting technique appears in table 6. In all tests (both for control and retrofitted specimens) no damage of the stirrups was observed, with their ends remaining closed.

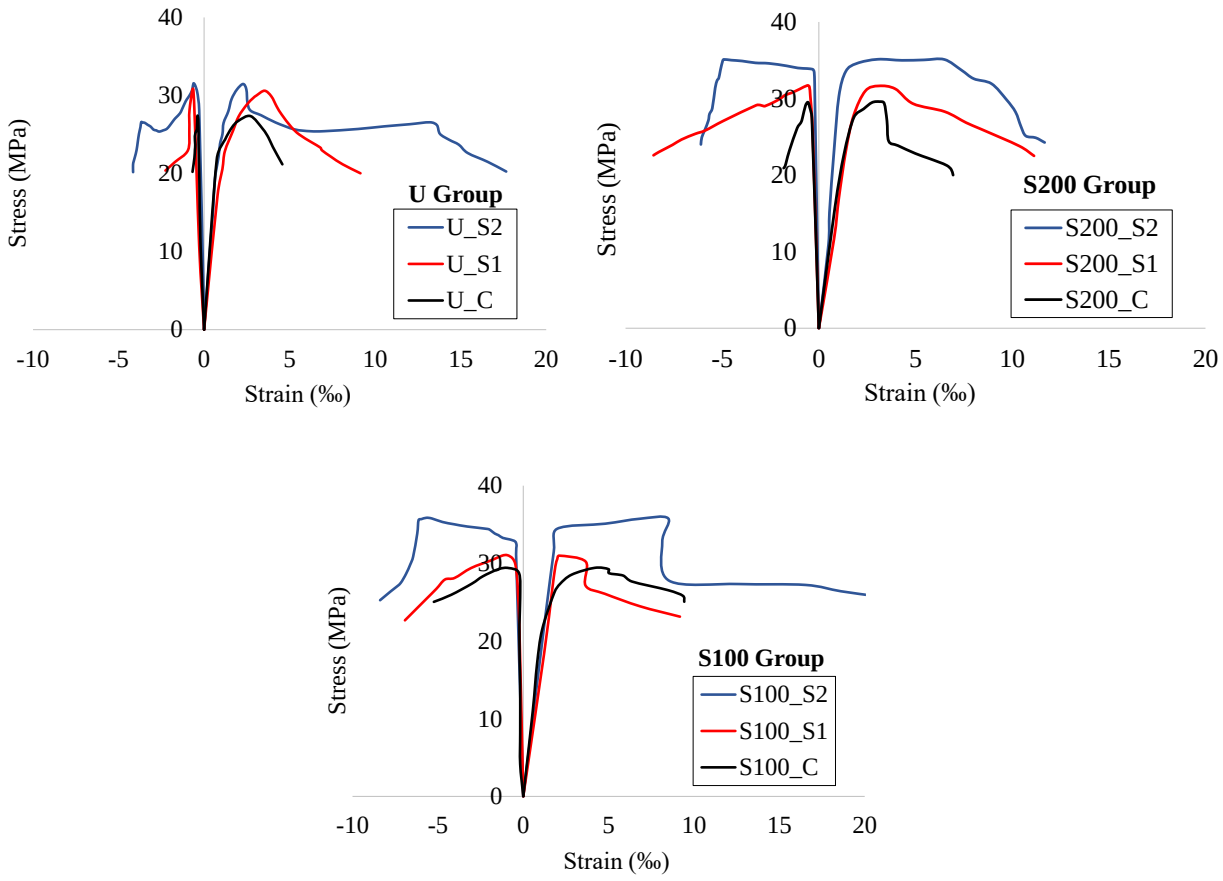

Figure 5. Experimental comparison between axial and lateral stress-strain curves for specimens of each group.

Table 5. Experimental failure modes of SRG jackets and longitudinal reinforcement of retrofitted specimens.

	U Group		S200 Group			S100 Group		
Specimen	**U_S1**	**U_S2**	**S200_C**	**S200_S1**	**S200_S2**	**S100_C**	**S100_S1**	**S100_S2**
Failure Mode of SRG Jacket	Debonding	Mixed	-	Debonding	Mixed	-	Debonding	Mixed
Buckling	-	-	Moderate	Moderate	Intense	No	Moderate	Intense

Table 6. Strength, strain, and energy dissipation increase for each retrofitted specimen, compared to the control one of the corresponding group.

	U_S1	**U_S2**	**S200_S1**	**S200_S2**	**S100_S1**	**S100_S2**
σ_{max}	11.8 %	15 %	7.4%	18.9 %	5.7%	22.1 %
$\varepsilon_{ult}/\varepsilon_{max}$	22.6 %	302.4 %	63.8 %	167.9%	241.6%	382.7 %
Energy	101.7%	302.3%	75.6%	138.3%	3.6%	113.1%

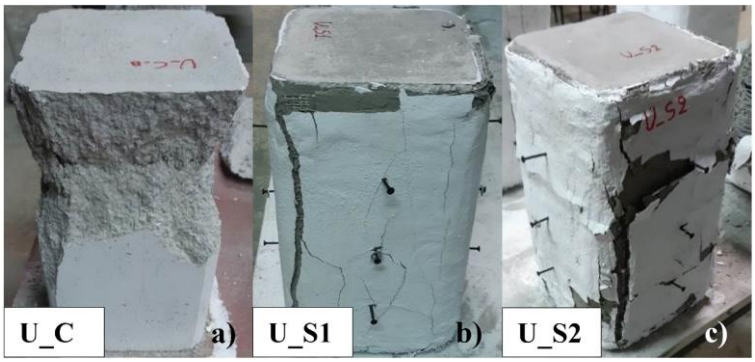

Figure 6. Experimental failure mode of the group U (plain concrete) specimens. a) Failure of the control specimen; b) Debonding of the single-layer jacket; c) Partial debonding of the outer layer of the double-layer jacket.

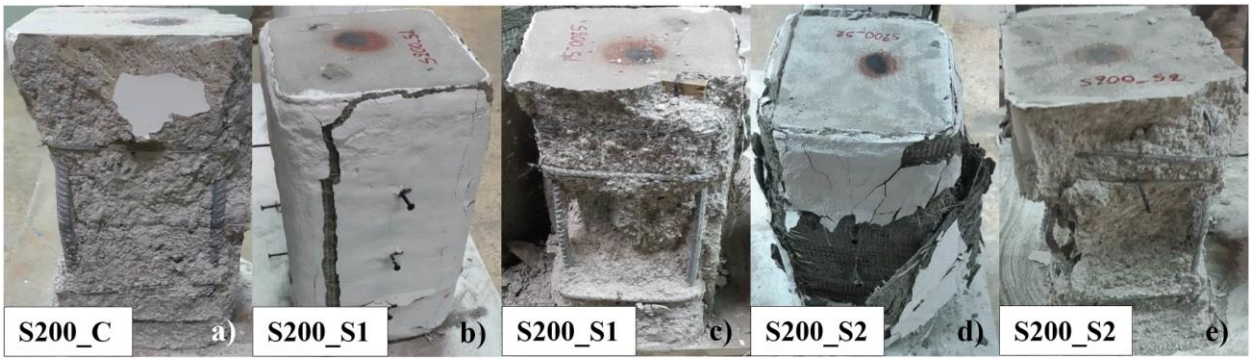

Figure 7. Experimental failure mode of the S200 specimens. a) Failure mode of the non-jacketed specimen; b) Debonding of the single layer jacket; c) Failure of the concrete core and moderate reinforcement buckling for the single-layered specimen; d) Partial debonding of the outer layer of the two-layer jacket; e) Failure of the concrete core and significant reinforcement buckling for the double-layered specimen.

Figure 8. Experimental failure mode of the specimens of group S100. a) Failure mode of the core; b) Debonding of the SRG jacket; c) Failure of the concrete core and moderate reinforcement buckling; d) Partial debonding of the two layers of SRG jacket; e) Failure of the concrete core and intense reinforcement buckling.

4. NUMERICAL MODELING

This section describes a finite element procedure for predicting the response of SRG-retrofitted columns in axial compression. The objective of the numerical model is to provide an effective and practical methodology to predict the response of SRG-confined RC columns under compression. Such a methodology can supplement the existing analytical equations [41,43,48] and facilitate the design and analysis procedure of SRG-retrofitted RC structures. Towards this direction, three-dimensional finite elements and inelastic material constitutive laws were utilized,

whereas a recently published methodology [62] for modeling external jackets is applied. Finite element software ATENA [68-70] was selected, based on the following advantages [71]:

a. Availability of a robust and mesh-independent nonlinear constitutive model for concrete.

b. Ability to model steel reinforcement using embedded (instead of discrete) truss elements.

c. Availability of reliable convergence algorithms and nonlinear solvers for deriving the softening branch of the compressive response.

The numerical results were compared to the experimental ones based on the following criteria:

i) Similarity between experimental and numerical failure modes, both for the concrete core and SRG jacket.

ii) Prediction of the failure modes and the resulting axial and lateral response curves (stress vs. strain). Specifically, the model should predict the maximum stress (σ_{max}) and the corresponding axial and lateral strain ($\varepsilon_{max,axial}$ and $\varepsilon_{max,lateral}$) as well as the ultimate stress (σ_u) and the corresponding axial and lateral strain ($\varepsilon_{u,axial}$ and $\varepsilon_{u,lateral}$). The final comparison parameter was the energy dissipation capacity of the column, which corresponds to the area below the corresponding response curve.

Previous studies [61] and software guides [70] suggest the use of two-dimensional (plane stress) elements to model externally applied composite jackets. This approach considers the R/C member (modeled with 3D solid elements), the external jacket (modeled with 2D plane stress elements), and an auxiliary surface (between the concrete member and the external jacket). The concrete core is connected to this auxiliary surface using a fixed contact, whereas the auxiliary surface is connected to the external jacket using an interface volume element. This auxiliary surface has no physical meaning; it is only utilized to make the meshes of the R/C member and the textile compatible [70]. Trial analyses proved that this approach is linked to several drawbacks, such as complexity, time-inefficiency, and, most importantly, the inability to accurately predict

the experimentally observed behavior. The main shortcomings of this approach are summarized in [62]. This study adopts a new approach for modeling SRG jackets, where steel cords are individually represented by 2-node truss elements embedded in the concrete volume. This method was proved as accurate and time-efficient in modeling SRG-retrofitted R/C beams [62].

4.1 Material constitutive laws

4.1.1 Concrete

A confinement-sensitive three-dimensional combined fracture-plastic material model (NonLinCementitious3) was selected for concrete [73-77]. This constitutive law is suitable for practical applications since it is effectively defined by a single parameter; concrete compressive strength (f_c). Following the experimental investigation, the compressive strength was set to f_c = 24.1 MPa. To completely characterize the numerical model, the following parameters are calculated: tensile strength (f_t), fracture energy (G_f), modulus of elasticity (E_c), Poisson ratio (ν), eccentricity (e), onset on concrete crushing (σ_{co}), multiplier of tensile strength (λ_t), threshold of plastic volumetric strain ($\varepsilon_{v,t}{}^P$), softening parameter (t_s), plastic potential order (n), and three plastic potential parameters (A, B, C). The values of these parameters (Table 7) were calculated based on analytical equations using the concrete strength as the only input. The reader may refer to [71] for the corresponding equations and to [73-77] for the detailed description of the numerical model.

The utilized material law treats fracture in tension based on the orthotropic smeared crack formulation (crack band approach) which takes into account strain localization, using the Rankine failure criterion with exponential softening. In compression, the Menétrey-Willam [78] failure surface is employed, with the plastic volumetric strain as a hardening/softening parameter and a non-associated flow rule based on a nonlinear plastic potential function. The model can simulate phenomena such as concrete cracking, crushing under high confinement and crack closure due to crashing in other directions. It is noted that the adopted confinement-sensitive material model

accounts automatically for the strength and ductility increase of concrete due to confinement, through the interaction with the stirrups and the aforementioned material law. The accuracy of the utilized model was assessed in the past through an extensive parametric study of circular and rectangular bridge piers of solid and hollow section [75,76]. The present application is the first one to use this constitutive law to model *retrofitted* columns under concentric compression.

Table 7: Summary of the concrete parameters used in the numerical study.

Parameter	f_c **(MPa)**	f_t **(MPa)**	G_f **(MN/m)**	E_c **(GPa)**	ν **(-)**	**e (-)**	σ_{co} **(MPa)**
Value	24.1	2.1	5.5×10^{-5}	25.8	0.2	0.52	6.1
Parameter	λ_t **(-)**	$\varepsilon_{v,t}^{P}$ **(-)**	t_s **(-)**	**n (-)**	**A (-)**	**B (-)**	**C (-)**
Value	1.124	5.6×10^{-4}	1.61×10^{-3}	3	6.73	-9.19	-47.5

4.1.2 Steel Reinforcement

The constitutive law utilized for reinforcement is based on a uniaxial multilinear law, enabling a description of all stages of steel behavior, both elastic and inelastic. A bilinear stress-strain diagram, corresponding to the experimental data of steel grade B500C was selected. The yield stress, the maximum stress, the yield strain, and the strain at maximum stress being equal to f_y = 587 MPa, f_{max} = 651 MPa, ε_y = 0.0029, and ε_{max} = 0.11 (Figure 9, left). The reinforcement was embedded in the concrete volume. A perfect bond (zero-slip) between internal steel reinforcement and concrete was assumed since sufficient anchorage length was provided.

4.1.3 Steel-reinforced grout

SRG cables were represented individually (one-by-one) as embedded elements in the concrete volume, using a similar constitutive law to reinforcement. Given that the density of the textile utilized in the experimental investigation was 3.15 cords/cm and that the retrofitted height of the columns was 36 cm, a total of 113 individual cords along the height of the specimen was modeled. According to the manufacturer, the stress-strain diagram of the steel cords is bilinear, with a

maximum stress of σ_{max} = 2800 MPa and a corresponding strain of ε_u = 0.01474 (Figure 9, right). The modulus of elasticity of the steel cords is E = 190 GPa. This stress-strain response was assigned to the embedded elements adopted in the numerical model. The minor tensile strength of the inorganic matrix was ignored, and its effect (adhesion between cords and the R/C beam) was indirectly considered. In specimens where two layers of SRG jacket were utilized (specimens U_S2, S200_S2, and S100_S2), perfect bond (zero-slip) between the cords of the inner layer and the column was adopted. The *fib* MC 2010 [72] bond-slip law was applied on the endpoints of the cords, in the single-layered specimens (U_S1, S200_S1, and S100_S1) and in the outer layer of SRG, in the double-layered specimens, where slippage is expected to occur. From the available options in *fib* MC 2010 [72], the bond was considered as "Good," and the corresponding values were selected. It is noted that no additional interaction is considered between the inner and the outer SRG layers in double-layered specimens.

It is noteworthy that the adopted bond-slip law is a simplification of the physical problem, aiming at promoting the robustness of the modeling process. Any bond behavior between the fibers and the matrix, as well as the matrix and the substrate, is now *smeared* into the adopted bond-slip law, which describes these phenomena macroscopically. The *fib* MC 2010 [72] bond-slip model was employed due to the lack of a specialized bond-slip law derived for SRG steel cords. The numerical results, as described in the next section of the present paper, show that this initial assumption was reasonable. More details regarding the selected bond-slip law and the adopted parameters appear in [62].

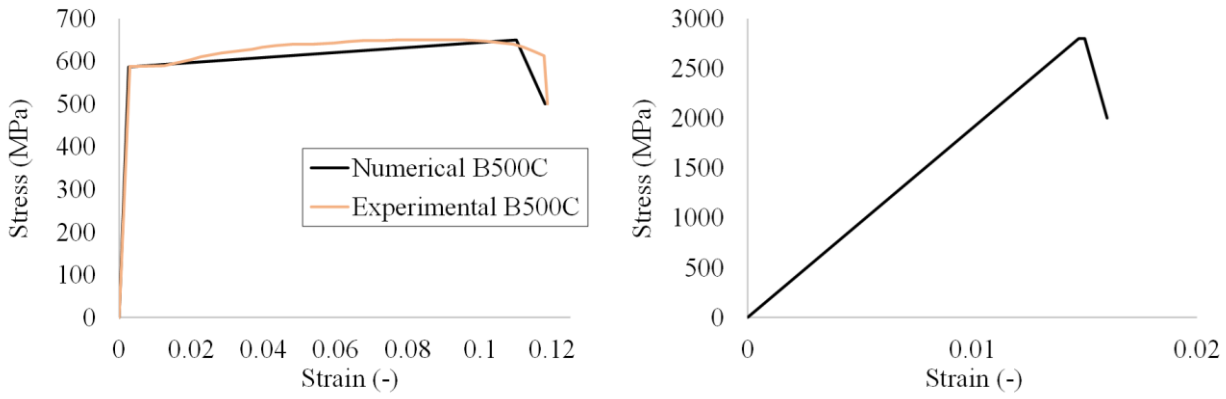

Figure 9. Stress-strain diagram. Left) Internal steel reinforcement; Right) Steel cords of the SRG jacket.

4.2 Finite element modeling and analysis procedure

Concrete was modeled using 8-node isoparametric solid (brick) elements, with three degrees of freedom per node, comprising eight integration points, with each side length equal to 17 mm. Trial parametric studies showed that a finer mesh neither increases accuracy nor is recommended, because it falls below the maximum aggregate size (8 mm). Steel cables and reinforcement were modeled by 2-node truss elements, with one axial degree of freedom per node and two integration points, embedded in concrete elements.

The load was applied as prescribed displacement in small increments to simulate the experimental procedure and favor convergence. Five monitoring points were utilized to obtain the stress-strain curves of the specimens, similarly to the experimental procedure. The first was placed in the loading plate and monitored both the applied load, essentially the reaction of the column to the prescribed displacement, and the corresponding axial displacement. The remaining four monitoring points were placed in the middle of the height of the specimen and measured the lateral displacement (expansion). Displacements were converted into strains and load into stress, using

the same procedure utilized to convert the experimental measurements, as described in a previous section.

4.3 Convergence criteria

The modified Newton-Raphson (mNR) iterative scheme was applied, with appropriate convergence criteria and a maximum number of iterations. The displacement error, the residual error, and the absolute residual error were equal to 0.005, energy error was equal to $5 \cdot 10^{-6}$, and the maximum number of iterations was set to 200. An elastic predictor was selected (no stiffness updates through iterations), whereas the stiffness matrix was assembled at each step. From the various available solvers, Pardiso [79] was chosen. The efficiency of this set of parameters was evaluated through previous studies [75,76]. Moreover, trial parametric analyses proved that further refinement of the parameters mentioned above (e.g. finer stepping) does not increase the accuracy of the results but only leads to a longer solution time.

5. NUMERICAL RESULTS

Control specimens (U_C, S200_C, S100_C) and specimens retrofitted with *one layer of SRG jacket* (U_S1, S200_S1, and S100_S1) had a bilinear stress-strain response, which was accurately captured by the numerical analysis (Figures 10, 11). The point of maximum stress coincides with concrete cracking (Figure 12a) and the debonding of the jacket, for the control and the single-layered specimens, respectively. For the single-layered specimens, the descending branch of the bilinear graph was milder. This is because, even after debonding, the SRG layer received (low) tensile stresses (Figure 12b).

Specimens retrofitted *with two layers of SRG jacket* had a plateau in their stress-strain response, which initiated after the maximum stress is reached (when debonding of the outer SRG layer initiates) and ended at the point of fracture of the cords of the inner layer of SRG. This plateau

was directly captured for specimen U_S2 and indirectly captured for specimens S200_S2 and S100_S2 through the mildly descending post-peak branch of the numerical graph (Figure 10, 11).

Figure 10 compares the experimental and numerical results, with the left and right part of the plot showing the lateral and axial strain, respectively. Figure 11 compares the experimental and the numerical results for the main response quantities (σ_{max}, $\varepsilon_{max,axial}$, $\varepsilon_{max,lateral}$, σ_u, $\varepsilon_{u,axial}$, $\varepsilon_{u,lateral}$ and dissipated energy), together with the corresponding correlation coefficients.

The *failure modes* captured by the numerical analysis include the cracks and stresses of the concrete core, the tensile stress of the external SRG layers (before and after debonding), and the tensile stress of the inner SRG jacket up to fracture.

The numerical analysis accurately predicted the failure mode of the *control specimens* with cracks in the middle of the height of the column. As the applied load increased, the crack width increased as well, and more areas failed due to excess concrete tensile strength, which is equal to 2.1 MPa (Figure 12a). In areas near the loading plates, principal stresses were mainly compressive, avoiding tensile failure. Figure 12a shows a typical concrete failure, as predicted by the numerical analysis.

In specimens *retrofitted with one layer of SRG jacket*, debonding of the jacket was captured by the utilized *fib* MC bond-slip model [72]. As loading proceeds, both the stresses of the SRG cords and the reaction force of the specimen increase. When the specimen reaches its maximum strength, the cords reach a tensile stress that is roughly equal to 300 MPa, and subsequently, slippage occurs (Figure 13). This stress level (300 MPa) is the upper limit that the steel cords can reach in this group of specimens. Hence, only a small part of the tensile strength of the cords is exploited, since the response is mainly governed by the anchorage length. Debonding of the jacket leads to a reduction of the tensile stresses of the cords and of the overall bearing capacity of the column. After the initiation of debonding the jacket maintains a part of its strength, receiving

stresses in the range of 235 MPa (Figure 11b). These numerical results are consistent to the visual observations during experimental testing where load drop coincided with the debonding of the jacket.

In specimens *retrofitted with two layers of SRG jacket*, the numerical analysis accurately captured the response of both inner and outer SRG layers. The outer SRG layer failed due to debonding, with a mechanism identical to the one described above for the single-layered specimens (Figure 12d). This is because these layers are characterized by the same bond-slip law (*fib* MC 2010 [72]), as described in detail in section 4.1.3. Debonding occurred with the outer steel cords having a stress of 300 MPa at the peak stress of the specimen (Figure 13). Right after debonding, load drop was observed, the stresses of the inner SRG layer increased, whereas stresses of the outer one decreased, reaching a residual stress of 235 MPa (Figures 12b, 13). The column maintained a significant part of its bearing capacity due to the additional confinement provided by the inner SRG layer. The inner SRG layer failed at the maximum strength of 2800 MPa (Figure 12c) when the column reached its ultimate strength. The failure modes of both the outer layer (debonding at maximum strength of the specimen) and the inner layer (tensile fracture at the ultimate strength of the specimen) are consistent to the experimental observations described in section 3.

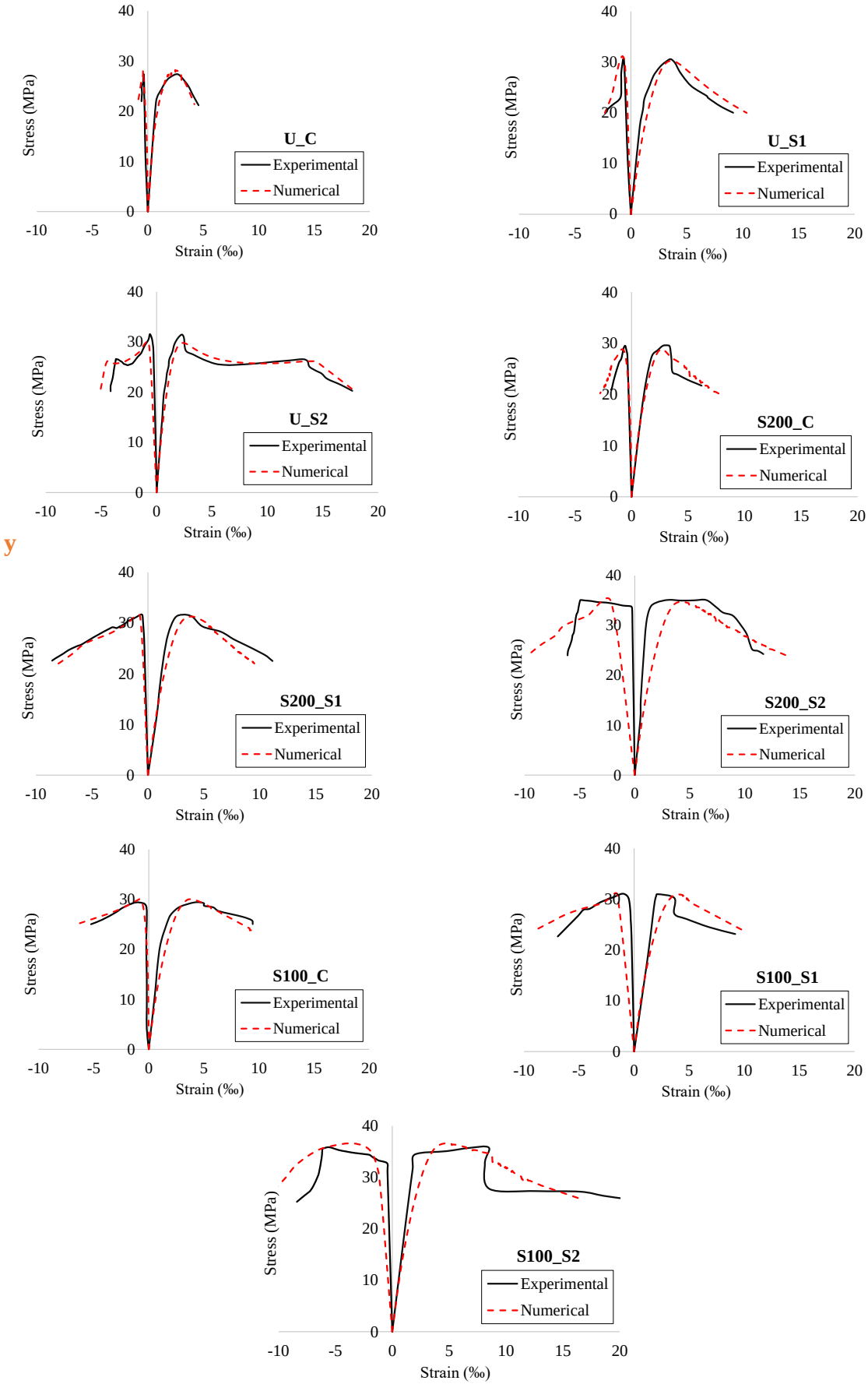

Figure 10. Comparison of experimental and numerical stress-strain curves.

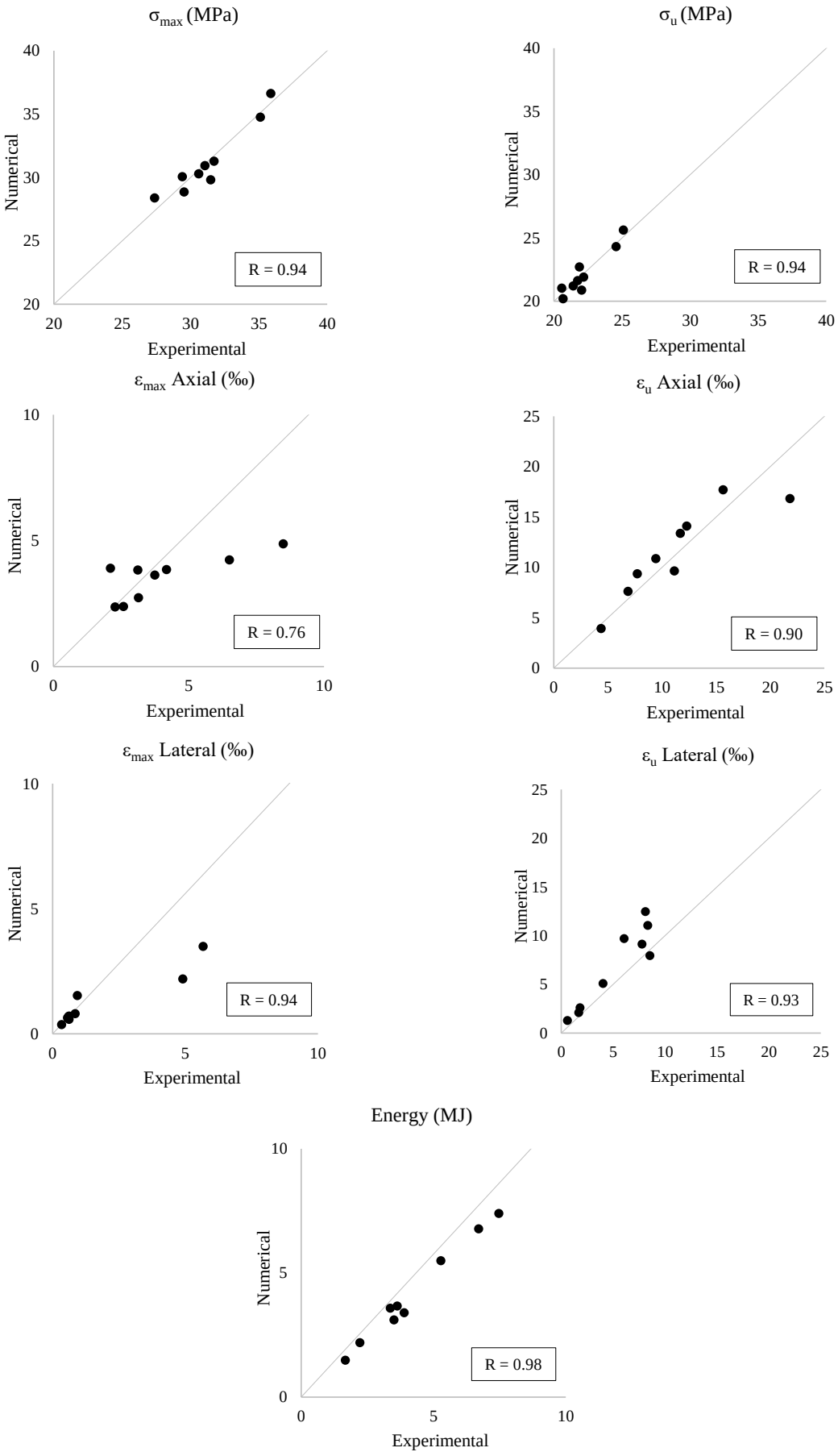

Figure 11. Comparison between experimental and numerical results for the main response quantities.

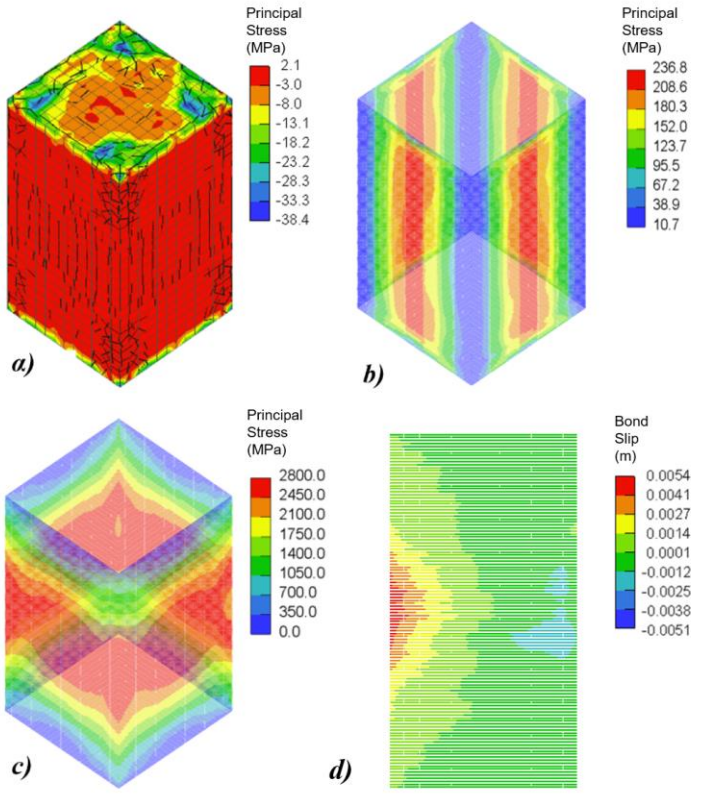

Figure 12. Numerical failure modes. a) Concrete cracking; b) Tensile stress of the external layer of SRG jacket at failure; c) Tensile stress of the internal layer of SRG jacket at failure; d) Slippage of the external layer of SRG at failure.

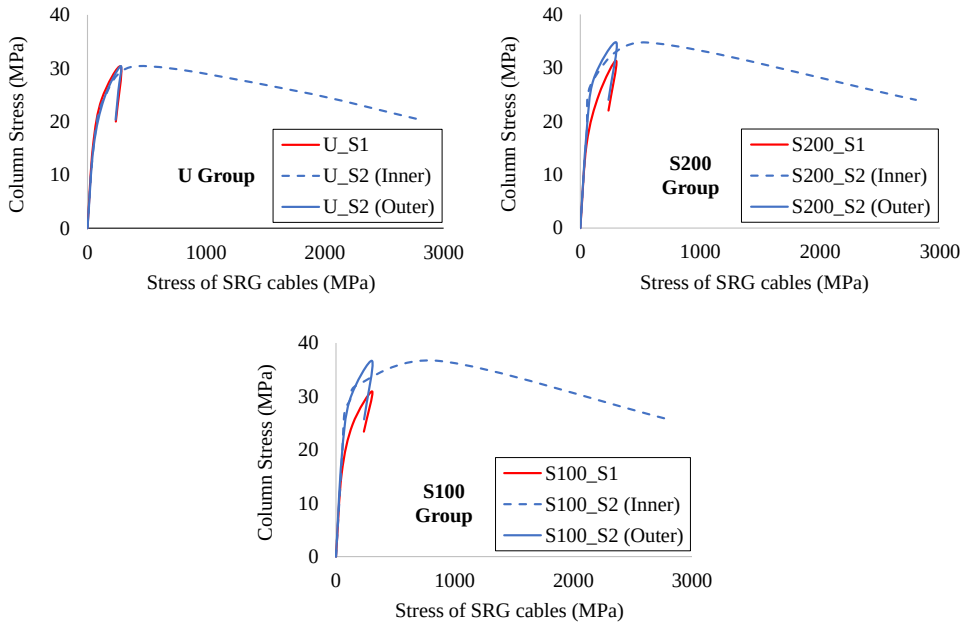

Figure 13. Developed stresses in the SRG cables versus the axial stress of the columns, as predicted by the numerical analysis.

Figure 13 summarizes the stresses of the SRG cables in comparison to the axial stress of the column, as predicted by the numerical analysis. The axial stress of the column (noted as "Column Stress" in Figure 13) is equal to the one plotted in the vertical axis of Figure 10. As described above, both the SRG layer of the single-layered specimens, and the outer SRG layer of the double layered specimens, exhibit a similar response (i.e., the values of the horizontal axis of Figure 13 are practically identical). These layers reach a maximum stress of approximately 300 MPa and maintain a stress of approximately 235 MPa at failure. As the double-layered specimens tend to have higher axial strength (mainly evident in groups S200 and S100), the vertical axis of the corresponding graphs reaches higher values. The inner SRG layers in double-layered specimens reach a maximum stress of 2800 MPa at the ultimate stress of the column, which is evident in the right-most point of the graphs (Figure 13). After failure of the inner SRG layer, the column loses its bearing capacity.

The main limitation of the proposed numerical methodology is the inability to capture the buckling mode of the internal longitudinal steel reinforcement. This is because the longitudinal bars are modeled with truss elements, which operate only axially (in tension and compression). This implies that buckling, which is inherently three-dimensional, is a phenomenon beyond the range of truss elements. The above limitation was also acknowledged in previous studies, where the importance of the bar buckling was not considered as critical [75,76]. In the present study, buckling was pronounced in two out of nine specimens, namely, specimens S200_S2 and S100_S2. These are the two specimens where the largest deviation between the numerical and the experimental stress-strain curve was observed. However, when the numerical methodology is assessed based on its ability to predict the overall stress-strain response, and not each specific point of the curve, the correlation is satisfactory, even for these specimens (Figure 10).

Moreover, through the use of truss elements for the internal reinforcement, the model does not account for the limited (yet non-zero) bending stiffness of the longitudinal steel reinforcement.

Previous studies suggest that this bending stiffness can be neglected in most practical applications [e.g., 71]. These effects (buckling and bending stiffness), in addition to the variability of the concrete properties, could explain the apparent deviation between the experimental and the numerical initial (elastic) branch of the lateral stress-strain curve (e.g., specimen S100_S1, Figure 10).

6. PROPOSED DESIGN AND ANALYSIS PARAMETERS

The present section summarizes the suggested design criteria, manufacturing parameters of consideration, as well as the proposed numerical methodologies, based on the experimental and the numerical results of the present paper.

The experimental results proved that the strength and the deformability of RC columns can be substantially enhanced when the SRG cords fail in tensile fracture. This conclusion promotes design and manufacturing solutions that lead to avoidance of debonding. Towards this direction, the following practical directions are suggested:

a. Using more than one layer of SRG, since the outer layer operates as an additional anchorage for the inner. Alternatively, a single layer of SRG jacket, with sufficiently long anchorage length or additional mechanical measures, could be employed.

b. Using low-density steel fabrics to facilitate installation and penetration of the cords in the mortar matrix. It is recommended that future practical applications use fabric densities that are close to, or lower than, the density of the present study (3.15 cords/cm).

c. Pre-bending of the steel fabrics before installation, especially for fabrics with density similar to the one employed in the present study.

Based on the close correlation between the numerical and the experimental results, the following numerical methods are proposed:

a. Explicit modeling of each individual steel cord of the SRG jacket using 2-node truss elements, instead of “equivalent” plane stress elements for the whole layer of SRG. The truss elements are embedded in the concrete volume. The zero-slip approach for the fully anchored SRG layers, and the *fib* MC 2010 [72] bond-slip law are adequately accurate approaches for the description of the bond behavior of the cords, in the absence of a more refined bond-slip law.

b. Employing a confinement-sensitive three-dimensional combined fracture-plastic material model for concrete. Such a material can accurately capture the confinement effect originating both from the SRG jacketing and the internal stirrups. This material law can be assigned to 8-node isoparametric solid (brick) elements, providing accurate results.

c. Using 2-node truss elements, embedded in the concrete volume, to simulate internal steel reinforcement. These elements can describe the response of the longitudinal reinforcement, as well as the confinement effect provided by the stirrups, with sufficient accuracy.

7.CONCLUSIONS

In this paper, a systematic experimental and numerical investigation of the uniaxial compression behavior of SRG-retrofitted column-type specimens is presented. Nine specimens with different internal steel reinforcement and SRG strengthening configurations were tested under monotonic uniaxial compression. Experimental results demonstrated that strength and ductility increase in the jacketed specimens was significant, especially in the specimens retrofitted with two layers of SRG jacket. Numerical simulations were performed, using advanced three-dimensional constitutive laws for the involved materials, with the present study being the first to model SRG-retrofitted R/C columns using three-dimensional finite elements. The close correlation between the numerical and experimental results proved the efficiency of the proposed model. Based on the results of the study, the following conclusions are drawn:

- Single-layered columns failed due to jacket debonding (semi-ductile failure mode). Double-layered columns failed due to combined failure mode, that is, debonding of the external layer and tensile fracture of the inner one (ductile failure mode) (Figures 6-8). Both failure modes occurred at the point of maximum stress of the stress-strain curve. In all applications, the density of the SRG textile was equal to 3.15 cords/cm and the anchorage length equal to two sides of the column (i.e., 400 mm).
- SRG jacketing configurations managed to increase the maximum stress (σ_{max}), axial strain ratio ($\varepsilon_{ult} / \varepsilon_{max}$), and dissipated energy up to 22.1%, 302.3%, and 382.7%, respectively. These values validate the efficiency of the implemented SRG jacketing configurations, with the stress, ductility and energy dissipation increase being more significant when two layers of SRG jacket are utilized.
- The influence of the internal steel reinforcement was evaluated. For plain concrete specimens or for columns with sparse stirrups, the strength and ductility gain from retrofitting was higher (Table 6). Hence, the qualitative assumption is that for higher internal steel reinforcement, the effect of the retrofitting is less significant.
- Numerical and experimental failure modes were closely correlated both for the R/C column and the SRG jacket (Figures 6-8,12,13). The analysis predicted the concrete failure and the crack concentration in the middle of the height of the column, as well as the failure mode of the jacket. Debonding of the jacket in single-layered specimens or of the outer layer in double-layered specimens was accurately predicted using the *fib* MC [72] bond-slip model (Figure 12). In specimens retrofitted with two layers of SRG jacket, the fracture of the steel cords of the inner layer was predicted, proving the suitability of the adopted full-bond (zero-slip) approach for those layers.
- The numerical analysis approximated the experimental stress-strain graphs closely (Figures 10, 11). The numerically obtained values for the maximum and ultimate stresses

(σ_{max}, σ_u), and the axial and lateral strains (ε_{axial}, $\varepsilon_{lateral}$) closely matched the experimental ones, proving the accuracy of the proposed methodology both in terms of strength and deformation. Dissipated energy, which is a more general indicator since it includes both stress and strain values, was also accurately predicted (Figure 11).

- The numerical analysis was less successful in capturing the buckling behavior of the longitudinal steel reinforcement. This is an inherent limitation of the 2-node truss elements that are commonly utilized to model internal longitudinal steel reinforcement. The experimental results showed that buckling is noteworthy only in specimens S200_S2 and S100_S1, where the maximum deviation between the experimental and the numerical stress-strain graph was observed. However, even in this case, the numerical stress-strain response still matches the experimental one with good accuracy.

The present study broadens the previously acquired knowledge on the compressive behavior of SRG-retrofitted RC columns, shedding more light in their structural behavior and the associated design parameters, employing both experimental and numerical techniques. Further experimental and numerical investigation of SRG-confined R/C columns is suggested, employing different internal steel configurations and alternative jacketing schemes. Finally, the development of a refined numerical bond-slip law for steel cords is also suggested.

Acknowledgments

Special thanks are attributed to Interbeton and Kerakoll S.p.A. for providing the materials for the experimental investigation. Mr. Konstantinos Mixios is kindly acknowledged for his assistance during the preparation of the experimental campaign.

References

[1] Bakis C.E., Bank L.C., Brown V.L., Cosenza E., Davalos J.F., Lesko J.J., Machida A., Rizkalla S.H. and Triantafillou T.C. (2002) "Fiber-Reinforced Polymer Composites for Construction – State-of-the-Art Review" Journal of composites for construction DOI: 10.1061/(ASCE)1090-0268(2002)6:2(73)

[2] Triantafillou T.C. (1998) "Shear Strengthening of Reinforced Concrete Beams Using Epoxy-Bonded FRP Composites" ACI Structural Journal, 95, 107-115

[3] Triantafillou T.C., Choutopoulou E., Fotaki E., Skorda M., Stathopoulou M., Karlos K. (2015) "FRP confinement of wall-like reinforced concrete columns" Materials and Structures DOI 10.1617/s11527-015-0526-5

[4] Kotynia, R., Baky, H.A., Neale, W., Ebead, U.A. (2008) "Flexural Strengthening of RC Beams with Externally Bonded CFRP Systems: Test Results and 3D Nonlinear FE Analysis", Journal of Composites for Construction, https://doi.org/10.1061/(ASCE)1090-0268(2008)12:2(190)

[5] Triantafillou T.C., Deskovic N., Deuring M. (1992) "Strengthening of Concrete Structures with Prestressed Fiber Reinforced Plastic Sheets" ACI Structural Journal, Title no. 89-S22

[6] Sneed, L.H., Ravazdezh, F., Santandrea M., Imohamed, I.A.O., Carloni, C. (2017) "A study of the compressive behavior of concrete columns confined with SRP jackets using digital image analysis", Composite Structures, https://doi.org/10.1016/j.compstruct.2017.07.047

[7] Triantafillou T.C., Plevris N. (1992) "Strengthening of RC beams with epoxy-bonded fibre-composite materials" Materials and Structures, 1992, 25, 201-211

[8] Tastani S.P., Pantazopoulou S.J., Zdoumba D., Plakantaras V., Akritidis E. (2006) "Limitations of FRP Jacketing in Confining Old-Type Reinforced Concrete Members in Axial Compression" Journal of Composites for Construction DOI: 10.1061/ASCE1090-0268(2006)10:1(13)

[9] Pantazopoulou S., Tastani S., Thermou G., Triantafillou T., Monti G., Bournas D., Guadagnini M. (2016) "Background to the European seismic design provisions for retrofitting RC elements using FRP materials" Structural Concrete, Ernst & Sohn, DOI: 10.1002/suco.201500102

[10] Ma G., Li H. (2015) “Experimental Study of the Seismic Behavior of Predamaged Reinforced-Concrete Columns Retrofitted with Basalt Fiber-Reinforced Polymer” J. Compos. Constr., 2015, 19(6): 04015016

[11] Lau D., Qiu Q., Zhou A., Chow C.L. (2016) “Long term performance and fire safety aspect of FRP composited used in building structures” Construction and Building Materials 126 (2016) 573–585

[12] Koutas L. and Triantafillou T.C. (2013) “Use of Anchors in Shear Strengthening of Reinforced Concrete T-Beams with FRP” Journal of Composites for Construction 2013.17:101-107.

[13] Karatzikis M., Papanicolaou C.G., Antonopoulos C.P. and Triantafillou T.C. (2005) “Experimental Investigation of Nonconventional Confinement for Concrete Using FRP” Journal of Composites for Construction DOI: 10.1061/(ASCE)1090-0268(2005)9:6(480)

[14] Antonopoulos C.P. and Triantafillou T.C. (2003) “Experimental Investigation of FRP-Strengthened RC Beam-Column Joints” Journal of Composites for Construction DOI: 10.1061/(ASCE)1090-0268(2003)7:1(39)

[15] Mitolidis, G.J., Salonikios, T.N., Kappos, A.J. (2012) “Test results and strength estimation of R/C beams strengthened against flexural or shear failure by the use of SRP and CFRP”, Composites Part B: Engineering, https://doi.org/10.1016/j.compositesb.2011.11.034

[16] Antoniades, K.K., Salonikios, T.N., Kappos, A.J. (2005) “Tests on Seismically Damaged Reinforced Concrete Walls Repaired and Strengthened Using Fiber-Reinforced Polymers” Journal of Composites for Construction, https://doi.org/10.1061/(ASCE)1090-0268(2005)9:3(236)

[17] Mitolidis, G.J., Salonikios, T.N., Kappos, A.J. (2012) “Tests on RC Beams Strengthened at the Span with Externally Bonded Polymers Reinforced with Carbon or Steel Fibers” Journal of Composites for Construction, https://doi.org/10.1061/(ASCE)CC.1943-5614.0000281

[18] Antoniades, K.K., Salonikios, T.N., Kappos, A.J. (2005) “Tests on Seismically Damaged Reinforced Concrete Walls Repaired and Strengthened Using Fiber-Reinforced Polymers” Journal of Composites for Construction, https://doi.org/10.1061/(ASCE)1090-0268(2005)9:3(236)

[19] Antoniades, K.K., Salonikios, T.N., Kappos, A.J. (2007) “Evaluation of hysteretic response and strength of repaired R/C walls strengthened with FRPs”, Engineering Structures, https://doi.org/10.1016/j.engstruct.2006.11.021

[20] Koutas L., Triantafillou T.C. (2013) “Use of Anchors in Shear Strengthening of Reinforced Concrete T-Beams with FRP” Journal of Composites for Construction DOI:10.1061/(ASCE)CC .1943-5614.0000316.

[21] Thermou, G.E., Pantazopoulou, S.J. (2009) “Fiber-Reinforced Polymer Retrofitting of Predamaged Substandard RC Prismatic Members”, Journal of Composites for Construction

[22] Yuan H., Lu X., Hui D., Feo L. (2012) “Studies on FRP-concrete interface with hardening and softening bon-slip law” Composite Structures https://doi.org/10.1016/j.compstruct.2012.06.009

[23] Napoli A., Realfonzo R., Petracca M., Candeloro F., Camata G., Casadei P. (2016) “Flexural strengthening of RC slabs with SRP/SRG: an experimental-numerical comparison” Applied Mechanics and Materials doi:10.4028/www.scientific.net/AMM.847.381

[24] Napoli, A., Realfonzo, R. (2016) “Compressive behavior of concrete confined by SRP wraps, Construction and Building Materials”, https://doi.org/10.1016/j.conbuildmat.2016.01.055

[25] Triantafillou T.C., Papanicolaou C.G., Zissimopoulos P, Laourdekis T. “Concrete confinement with textile-reinforced mortar jackets” ACI Struct J 2006; 103(1): 28-37.

[26] Koutas L.N., Bournas D.A. (2016) “Flexural Strengthening of Two-Way RC Slabs with Textile-Reinforced Mortar: Experimental Investigation and Design Equations” Journal of Composites for Construction DOI: 10.1061/(ASCE)CC.1943-5614.0000713.

[27] Tetta Z.C., Koutas L.N., Bournas D.A. (2015) “Textile-reinforced mortar (TRM) versus fiber-reinforced polymers (FRP) in shear strengthening of concrete beams” Composites Part B: Engineering https://doi.org/10.1016/j.compositesb.2015.03.055

[28] Tetta Z.C., Koutas L.N., Bournas D.A. (2016) “Shear strengthening of full-scale RC T-beams using textile-reinforced mortar and textile-based anchors” Composites Part B: Engineering https://doi.org/10.1016/j.compositesb.2016.03.076

[29] Raoof S.M., Koutas L.N., Bournas D.A. (2017) “Textile-reinforced mortar (TRM) versus fibre-reinforced polymers (FRP) in flexural strengthening of RC beams” Construction and Building Materials https://doi.org/10.1016/j.conbuildmat.2017.05.023

[30] Raoof S.M., Koutas L.N., Bournas D.A. (2016) “Bond between textile-reinforced mortar (TRM) and concrete substrates: Experimental investigation” Composites Part B: Engineering https://doi.org/10.1016/j.compositesb.2016.05.041

[31] Bournas D.A., Lontou P.V., Papanicolaou C.G., Triantafillou T.C. (2007) “Textile-Reinforced Mortar versus Fiber-Reinforced Polymer Confinement in Reinforced Concrete Columns” ACI Structural Journal, 104-S70

[32] Koutas L.N., Tetta Z., Bournas D.A., Triantafillou T.C. (2019) “Strengthening of Concrete Structures with Textile Reinforced Mortars: State-of-the-Art Review” Journal of Composites for Construction DOI: 10.1061/(ASCE)CC.1943-5614.0000882

[33] Tetta, Z.C., Koutas, L.N., Bournas, D.A. (2018) “Shear strengthening of concrete members with TRM jackets: Effect of shear span-to-depth ratio, material and amount of external reinforcement” Composites Part B: Engineering https://doi.org/10.1016/j.compositesb.2017.10.041

[34] Bournas, D.A., Triantafillou, T.C., Zygouris, K., Stavropoulos, F. (2009) “Textile-Reinforced Mortar versus FRP Jacketing in Seismic Retrofitting of RC Columns with Continuous or Lap-Spliced Deformed Bars” Journal of Composites for Construction, https://doi.org/10.1061/(ASCE)CC.1943-5614.0000028

[35] Raoof, S.M., Bournas, D.A. (2017) “TRM versus FRP in flexural strengthening of RC beams: Behaviour at high temperatures” Construction and Building Materials, https://doi.org/10.1016/j.conbuildmat.2017.07.195

[36] Younis, A., Ebead, U., Shrestha, K.C. (2017) “Different FRCM systems for shear-strengthening of reinforced concrete beams” Construction and Building Materials, https://doi.org/10.1016/j.conbuildmat.2017.07.132

[37] Colajanni, P., Fossetti, M., Macaluso, G. (2014) “Effects of confinement level, cross-section shape and corner radius on the cyclic behavior of CFRCM confined concrete columns”, Construction and Building Materials, https://doi.org/10.1016/j.conbuildmat.2014.01.035]

[38] Gonzalez-Libreros, J., Zanini, M., Faleschini, A F., Pellegrino, C. (2019) “Confinement of low-strength concrete with fiber reinforced cementitious matrix (FRCM) composites”, Composites Part B: Engineering, https://doi.org/10.1016/j.compositesb.2019.107407

[39] Wakjira, TG, Ebead, U. (2019) “A shear design model for RC beams strengthened with fabric reinforced cementitious matrix” Engineering Structures, https://doi.org/10.1016/j.engstruct.2019.109698

[40] Wakjira, TG, Ebead, U. (2019) “Internal transverse reinforcement configuration effect of EB/NSE-FRCM shear strengthening of RC deep beams” Composites Part B: Engineering, https://doi.org/10.1016/j.compositesb.2019.03.004

[41] Thermou, G.E., and Hajirasouliha, I. (2018b) “Design-oriented models for concrete columns confined by steel-reinforced grout jackets” Construction and Building Materials, 178, 313-326.

[42] Thermou, G.E., Pantazopoulou, S. (2007) “Metallic fabric jackets: an innovative method for seismic retrofitting of substandard RC prismatic members” Structural Concrete, fib, pp. 35-46

[43] Thermou G.E., Katakalos K., Manos G. (2014) “Concrete confinement with steel-reinforced grout jackets” Materials and Structures DOI 10.1617/s11527-013-0239-6

[44] Thermou G.E., Katakalos K., Manos G. (2015) “Influence of the cross section shape on the behaviour of SRG-confined prismatic concrete specimens” Materials and Structures DOI 10.1617/s11527-015-0545-2

[45] Thermou G.E, Katakalos K., Alexiou G. (2016) “SRG jacketing of short RC columns: Experimental investigation” Greek Conference on Concrete Structures, Thessaloniki, November 2016

[46] Thermou G.E., Katakalos K., Manos G. (2018) “Experimental investigation of substandard RC columns confined with SRG jackets under compression” Composite Structures DOI:10.1016/j.compstruct.2017.09.082

[47] Thermou G.E., Papanikolaou V.K., Hajirasouliha I. (2021) “Structural performance of RC columns retrofitted with steel-reinforced grout jackets under combined axial and lateral loading” Engineering Structures, https://doi.org/10.1016/j.engstruct.2021.112946

[48] Thermou, G.E., and Hajirasouliha, I. (2018) “Compressive behaviour of concrete columns confined with steel reinforced grout jackets” Composites Part B: Engineering Journal, 138, 222-23.

[49] Thermou G.E., Katakalos K., Manos G. (2013) Influence of the loading rate of the axial compressive behaviour of concrete specimens confined with SRG jackets, COMPDYN 2013, 4th ECCOMAS Thematic Conference

[50] Thermou G.E., Papanikolaou V.K., Lioupis C., Hajirasouliha (2019) “Steel-Reinforced Grout (SRG) strengthening of shear-critical RC beams” Construction and Building Materials https://doi.org/10.1016/j.conbuildmat.2019.04.259

[51] Gonzalez-Libreros J.H., Sneed L.H., D’Antino T.D., Pellegrino C. (2017) “Behavior of RC beams strengthened in shear with FRP and FRCM composites” Engineering Structures 150 (2017) 830–842

[52] Wakjira G.T., Ebead U. (2019) “Experimental and analytical study on strengthening of reinforced concrete T-beams in shear using steel reinforced grout (SRG)” Composites Part B 177 (2019) 107368

[53] Wakjira G.T., Ebead U. (2020) “Shear span-to-depth ratio effect on steel reinforced grout strengthened reinforced concrete beams” Engineering Structures 216 (2020) 11037

[54] Katsamakas A.A., Mixios K.E., Papanikolaou V.K., Thermou G.E., Katakalos K.V. (2019) “A comparative experimental study of strengthened columns using steel reinforced grout (SRG) jacketing” SECED Conference 2019, Greenwich, London

[55] Larrinaga, P., Garmendia, L., Piñero, I., San-José, J.T. (2020) “Flexural strengthening of low-grade reinforced concrete beams with compatible composite material: Steel Reinforced Grout (SRG)”, Construction and Building Materials, https://doi.org/10.1016/j.conbuildmat.2019.117790

[56] Wakjira, TG, Ebead, U. (2021) “Strengthening of reinforced concrete beams in shear using different steel reinforced grout techniques” Structural Concrete. 2021; 22: 1113– 1127. https://doi.org/10.1002/suco.202000354

[57] De Santis, S., Ceroni, F., de Felice, G., Fagone, M., Ghiassi, B., Kwiecien, A., Lignola, G.P., Morganti, M., Santandrea, M., Valluzzi, M.R., Viskovic, A. (2017) “Round Robin Test on tensile and bond behaviour of Steel Reinforced Grout systems” Composites Part B: Engineering, https://doi.org/10.1016/j.compositesb.2017.03.052

[58] Ombres, L., Verre, S. (2019) “Flexural Strengthening of RC Beams with Steel-Reinforced Grout: Experimental and Numerical Investigation” Journal of Composites for Construction, https://doi.org/10.1061/(ASCE)CC.1943-5614.0000960

[59] Ascione, F., Lamberti, M., Napoli, A., Realfonzo, R. (2020) “Experimental bond behavior of Steel Reinforced Grout systems for strengthening concrete elements” Construction and Building Materials, https://doi.org/10.1016/j.conbuildmat.2019.117105

[60] Malena, M., Sangirardi, M., de Felice, G. (2019) “Steel Reinforced Grout under uniaxial load: Experimental evidences and numerical modelling” Construction and Building Materials, https://doi.org/10.1016/j.conbuildmat.2019.116808

[61] Bencardino F. and Condello A. (2016) “3D FE Analysis of RC Beams Externally Strengthened with SRG/SRP Systems” MDPI Fibers 2016 4, 19 doi:10.3390/fib4020019

[62] Katsamakas A.A., Papanikolaou V.K., Thermou G.E. (2021) “A FEM-based model to study the behavior of SRG-strengthened R/C beams”, Composite Structures, https://doi.org/10.1016/j.compstruct.2021.113796

[63] Mau S. (1990) “Effect of tie spacing on inelastic buckling of reinforcing bars”. *ACI Structural Journal*. 87(6):671–7.

[64] fib bulletin 90. (2019) “Externally applied FRP reinforcement for concrete structures. Technical report, Task Group 5.1, *federation internationale du beton (fib)*

[65] Monti G, Nuti C. (1992) “Nonlinear cyclic behavior of reinforcing bars including buckling” *Journal of Structural Engineering* 118(12):3268–84.

[66] Pantazopoulou SJ. (1998) “Detailing for reinforcement stability in RC members” *Journal of Structural Engineering*, 124(6):623–32.

[67] Yalcin C, Saatcioglu M. (2000) “Inelastic analysis of reinforced concrete columns”. *Composite Structures* 77(5):539–55.

[68] Cervenka Consulting (2018) “ATENA Program Documentation”, Prague, Czech Republic.

[69] Červenka V., Jendele L., Červenka J. (2018) “Theory” ATENA Program Documentation Part 1, Červenka Consulting, Prague, Czech Republic.

[70] Sajdlová T. (2016) “ATENA Science – GiD Strengthening of concrete structures” ATENA Program Documentation Part 4-9, Červenka Consulting, Prague.

[71] Papanikolaou V.K. (2007) “Analytical Study of Confined Reinforced Concrete Members using the Three-Dimensional Nonlinear Finite Element Method” PhD Thesis, Aristotle University of Thessaloniki, Greece

[72] CEB-FIP Model Code 2010 (2010), Thomas Telford Ltd., London, 978-0-7277-1696-5

[73] Papanikolaou V.K., Kappos A.J. (2007) “Confinement-sensitive plasticity constitutive model for concrete in triaxial compression” International Journal of Solids and Structures, https://doi.org/10.1016/j.ijsolstr.2007.03.022

[74] Cervenka J., Papanikolaou V.K (2008) “Three dimensional combined fracture–plastic material model for concrete” International Journal of Plasticity, https://doi.org/10.1016/j.ijplas.2008.01.004

[75] Papanikolaou V.K., Kappos A.J. (2009) “Numerical study of confinement effectiveness in solid and hollow reinforced concrete bridge piers: Analysis results and discussion” Computers and Structures doi:10.1016/j.compstruc.2009.05.005

[76] Papanikolaou V.K., Kappos A.J. (2009) “Numerical study of confinement effectiveness in solid and hollow reinforced concrete bridge piers: Methodology” Computers and Structures doi:10.1016/j.compstruc.2009.05.004

[77] Papanikolaou, V., Kappos, A. (2005) “Modeling Confinement in Concrete Columns and Bridge Piers through 3D Nonlinear Finite Element Analysis” fib Symposium “Keep Concrete Attractive”, Budapest 2005

[78] Menétrey, P. and Willam K.J. (1995) “Triaxial Failure Criterion for Concrete and its Generalization”, ACI Structural Journal, Vol. 92, No. 3, pp. 311-318.

[79] Schenk O., Gärtner K., Fichtner W. and Stricker A. (2001) “PARDISO: a high-performance serial and parallel sparse linear solver in semiconductor device simulation” Future Generation Computer Systems, Volume 18, Issue 1, P 69-78, ISSN 0167-739X, https://doi.org/10.1016/S0167-739X(00)00076-5.